Detection of Vero Cells Infected with Herpes Simplex Types 1 and 2 and Varicella Zoster Viruses Using Raman Spectroscopy and Advanced Statistical Methods

Mahmoud Huleihel[1]*, Elad Shufan[2], Leila Zeiri[3], Ahmad Salman[2]*

1 Department of Microbiology, Immunology and Genetics, Faculty of Health Sciences, Ben-Gurion University of the Negev, Beer-Sheva, Israel, **2** Department of Physics, SCE- Shamoon College of Engineering, Beer-Sheva, Israel, **3** Department of Chemistry, Ben-Gurion University of the Negev, Beer-Sheva, Israel

* ahmad@sce.ac.il (AS); mahmoudh@bgu.ac.il (MH)

Abstract

Of the eight members of the herpes family of viruses, HSV1, HSV2, and varicella zoster are the most common and are mainly involved in cutaneous disorders. These viruses usually are not life-threatening, but in some cases they might cause serious infections to the eyes and the brain that can lead to blindness and possibly death. An effective drug (acyclovir and its derivatives) is available against these viruses. Therefore, early detection and identification of these viral infections is highly important for an effective treatment. Raman spectroscopy, which has been widely used in the past years in medicine and biology, was used as a powerful spectroscopic tool for the detection and identification of these viral infections in cell culture, due to its sensitivity, rapidity and reliability. Our results showed that it was possible to differentiate, with a 97% identification success rate, the uninfected Vero cells that served as a control, from the Vero cells that were infected with HSV-1, HSV-2, and VZV. For that, linear discriminant analysis (LDA) was performed on the Raman spectra after principal component analysis (PCA) with a leave one out (LOO) approach. Raman spectroscopy in tandem with PCA and LDA enable to differentiate among the different herpes viral infections of Vero cells in time span of few minutes with high accuracy rate. Understanding cell molecular changes due to herpes viral infections using Raman spectroscopy may help in early detection and effective treatment.

Introduction

One of the major causes of serious and life-threatening diseases in humans and animals are viruses. HSV-1, HSV-2 and VZV, which belong to the herpes family of viruses, are responsible for different human infections. They are mainly involved in painful and uncomfortable cutaneous infections; and in some cases can cause serious disorders such as blindness in the case of eye infection, and even death in the case of brain infections. That is in addition to their

involvement in serious genital infections [1]. Clinically, there is a high degree of similarity between the symptoms of infections from these viruses to those of bacterial or fungal infections. Therefore, it is very important to identify the cause of the infection rapidly and reliably, thereby enabling the physician to target the infection with the most appropriate treatment to avoid medical complications and side effects.

The routinely used detection assays of herpes viruses are cell culture, immunoassays [2] and molecular techniques which are usually time consuming and expensive. Apart from these conventional methods of herpes infection diagnosis [2, 3] there is a need to develop new approaches that are simple, objective, and noninvasive. Among the optical methods available, Raman spectroscopy has shown encouraging trends in the field of medicine. Raman spectroscopy is a noninvasive tool for studying biological systems that is well known for its simplicity and rapidity [4–7].

Analyzing biomolecules using Raman spectroscopy has become a promising tool for their detection and identification. Furthermore, there is no need for special sample preparation such as drying, labeling, or different fixation, which enables measuring biological samples with minimal manipulations and damage. The Raman technique has already been used for detection and identification of different kinds of cancers like melanoma [8], breast cancer [9, 10], squamous cell carcinoma [11], human coronary atherosclerosis [12], individual neoplastic and normal hematopoietic cells [13], uterine cervical cancer [14, 15], basal cell carcinoma [16], and skin cancer [17]. That is in addition to the identification of biochemical changes due to cell proliferation cultures [18, 19] and discrimination between normal and malignant cells in culture [20–25].

Raman shifts are characteristic to the vibrational molecular modes [26, 27] of the examined sample. The measured spectrum is considered as a 'biochemical fingerprint' because it contains bands that represent all molecules within the tested region of the sample [28]. The high spatial resolution of Raman spectroscopy (~ 1 μm) provides qualitative and quantitative information on the biochemical composition and structure of cells and tissues [29–32].

Various biomolecular components of the cell give a characteristic spectrum, which is rich in structural and functional aspects [22, 33]. The biochemical fingerprint of cells, tissues, and fluids that have been altered in a diseased state can be detected using Raman spectroscopy [34–39]. In our previous work [40] we used Raman spectroscopy followed by advanced statistical methods to successfully differentiate, with sensitivity approaching 100%, between a control group of Vero cells and another group of Vero cells that had been infected with HSV-1.

The main purpose of this work is to use Raman spectroscopy as an objective method for characterization and identification of Vero cells infected with herpes simplex viruses HSV-1, HSV-2, and VZV in cell culture. Cell cultures are considered as an advantageous and more convenient model for basic research [41, 42] when compared to "real" tissues, due to their homogeneity and the ability to control important culture parameters such as growth and malignant transformation rate. Cell cultures are used as a complementary method for studying the vibrational modes of normal and infected cells. The obtained Raman data will be studied focusing on the characteristic spectroscopic differences between the various herpes viral infections. These differences will then be used to identify and characterize the infected cells with each of the tested viruses.

Materials and Methods

2.1 Cells and viruses

African green monkey kidney (Vero) cells were obtained from the American Type Culture Collection (ATCC), Rockville, MD, USA. The cells were grown in RPMI medium containing 10% fetal calf serum (FCS), 1% glutamine, 50 U per ml penicillin, and 50 ug per ml streptomycin.

The ambient temperature was 37°C in humidified air containing 5% CO_2. Herpes viruses HSV-1, HSV-2, and VZV, were propagated to $> 10^9$ plaque forming units (PFU) per ml in Vero cells. Concentrations were estimated by plaque assay [43].

2.2 Cell infection and estimation of viral infection

Vero cells were plated at 0.20 million per well in 24 well culture plates in RPMI, with 10% FCS and antibiotics. After overnight incubation, the medium was removed and the wells were divided into four groups. Three of the four groups were infected, in RPMI containing 2% FCS for 2 hours at 37°C, by one of the three different viruses (HSV-1, HSV-2 and VZV), at a multiplicity of infection (m.o.i.) of 1. The fourth group was devoted as controls. The unadsorbed virus particles were removed and fresh medium containing 2% FCS was added, the monolayers thereafter incubated at 37°C. At 24 hours post infection the infected cells were examined by the following methods:

1. Raman spectroscopy

2. Morphological examination for the appearance of the cytopathic effect (CPE), which is defined as areas of complete destruction of cells or of morphologically modified cells are done by light inverted microscope. The percentage of damaged cells in the inspection field expresses the amount of the CPE

3. MTT test.

   In order to evaluate the number of living cells we used the MTT test. This test is an assay that examines the metabolic activity of the cells by measuring the reduction of 3-(4,5-dimethylthiazol-2-yl)-2,5-diphenol tetrazolium bromide (MTT) in the tested cells [44].

2.3 Sample Preparation

The cells were picked up from the tissue culture plates by treatment with trypsin (0.25%) for 2–3 minutes. The cells were centrifuged at 1000 rpm for five minutes. The pellet was washed twice with a physiologic solution (saline) and re-suspended in 100 µl of saline. The cells were counted by a hematocytometer, pelleted again by centrifugation, and re-suspended in an appropriate volume of saline to give a concentration of 40–50 cells per µl. Three microliters of the investigated cells were mounted on quartz slides and were measured in vitro using the Raman microscope after air drying for 15 minutes.

2.4 Raman measurements

A Jobin-Yvon (JY) LabRam HR 800 micro-Raman system with a liquid nitrogen cooled detector was used to carry out the Raman measurements in the 200–4000 cm^{-1} wavenumber region. Each measurement took 2 minutes to be performed. An argon laser (514 nm) was used for excitation, giving 3mW power on the sample. The specifications of the Raman system were determined to achieve about 4cm^{-1} spectral resolution. A 100 µm microscope with confocal hole and a microscope objective of x100 were used. A 600 grids per mm grating was set when performing the measurements. The measurements were performed over several weeks and the samples were prepared from different batches of cell cultures.

2.5 Spectral analysis

We tested 22 uninfected Vero cells, 21 cells infected with HSV-1 (Vero-HSV-1), 23 cells infected with HSV-2 (Vero-HSV-2), and 21 cells infected with VZV (Vero-VZV). All the

spectra were cut in the 600–1800 cm^{-1} region and were baseline corrected using concave rubberband correction after normalization with the vector normalization method, and then offset corrected using commercial OPUS 7 software.

2.5.1 Smoothing. Savitzky-Golay algorithm was used with 13 points in order to smooth the spectra. A small number of points were used to keep all the features of the Raman spectrum, without distortion of narrow bands.

2.5.2 Baseline correction. Concave rubberband correction algorithm was used for baseline correction. Using this method, the spectrum was divided into 64 ranges that have the same size. The minimum intensities in each range were calculated. A polynomial function was fitted using the calculated minima and was subtracted from the spectrum to achieve the baseline corrected spectrum.

2.5.3 Normalization. By using vector normalization, the average intensity at all wavenumbers of the spectrum is calculated and subtracted from the spectrum. The obtained spectrum is normalized to 1 by calculating the sum of the squares of all y-values, and dividing the spectrum by the square root of this sum. After performing vector normalization, some of the intensities of the spectrum are negative. Thus the all the vector normalized spectra were offset corrected by shifting the minimal intensities to zero.

2.6 Statistical analysis

Our objective was to analyze the Raman spectra of the measured cells to determine its type. The cell type belongs to one of the four categories—the control Vero, and three types of infected cells—Vero-HSV-1, Vero-HSV-2, and Vero-VZV. Each Raman spectrum includes D points (several hundreds)—Raman shift intensity as a function of wavenumber. In this study we acquired N = 217 measurements from the four categories. Each measurement is represented as a point in a D-dimensional space. PCA was used to reduce the number of dimensions, followed by LDA, which was used to detect characteristic features of each category [45–48].

2.6.1 LOO algorithm. The separation validation was carried out using the LOO algorithm. It is a common method of cross-validation that is used in case of a small-sized population. It has been extensively explored in machine learning. Using this method, the training set contains (N-1) measurements and one measurement is left out for validation. The procedure is repeated N times, and for each repetition a different measured spectrum is left out. All the measurements are used both for training and for validation with no randomness role. Using the LOO algorithm it is possible to calculate the average number of successes.

Results

Typical Raman spectra of control Vero cells, HSV-1, HSV-2, and VZV infected Vero cells, are presented in Fig 1 in the 600–1800 cm^{-1} wavenumber range. Each spectrum is an average of about 40 measurements taken from cells.

Proteins, lipids, nucleic acids, and carbohydrates are the main molecules that are included in all biological samples. The absorptions of these molecules' functional groups compose the Raman spectra of the four biological samples investigated in this study. Proteins are the main contributor to wavenumber region 1488–1726 cm^{-1}, due to amide I and II bands [49–52], with centroids at 1656 cm^{-1} and 1577 cm^{-1}, respectively. The peak centered at 1640 is attributed to amide I [53], while the peak centered at 1627 cm^{-1} is attributed to amide C = O, stretching vibration of β-form [54]. Phenylalanine, tyrosine aromatic portions, and to other proteins C = O stretching vibration [13, 55] attribute mainly to the shift bands at 1606 and 1618 cm^{-1}. Phenylalanine and hydroxyproline are the main contributors to the Raman band, due to the stretching vibration C—C, centered at 1580 cm^{-1}[56].
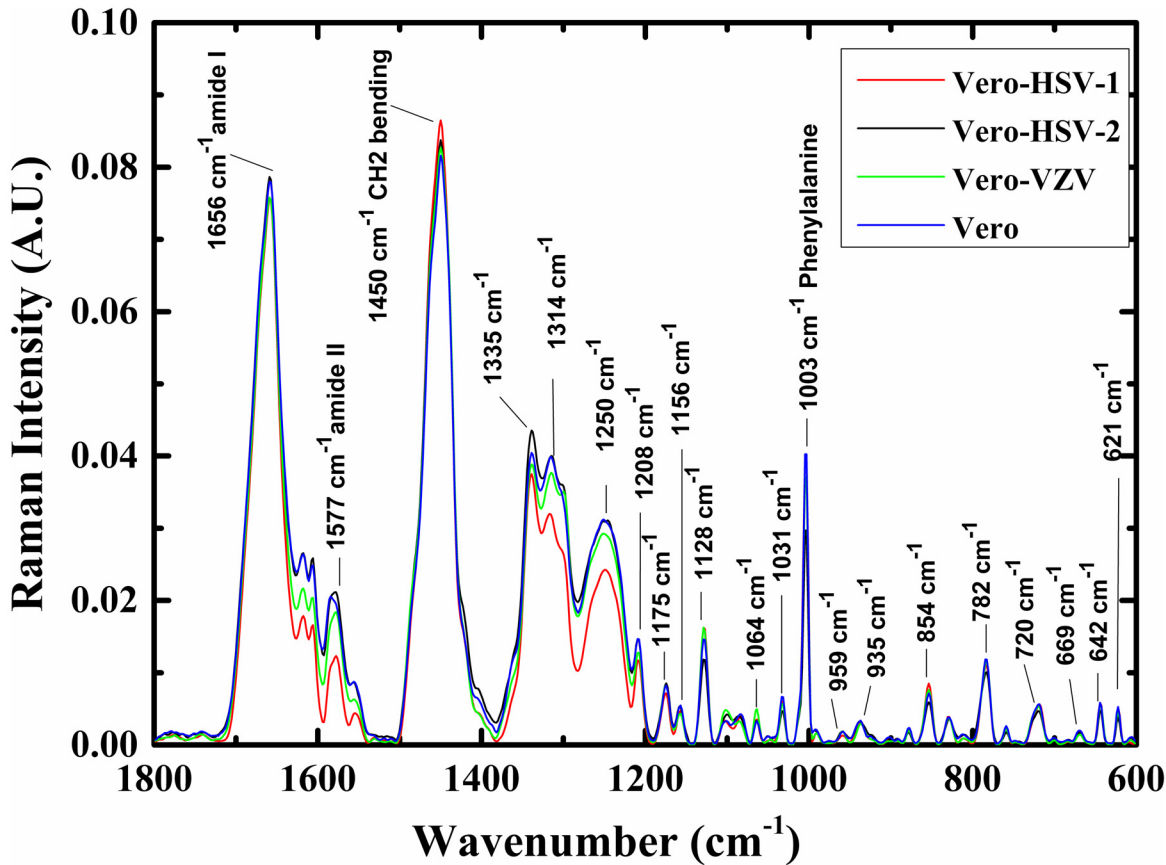
Fig 1. Average spectra of Raman shift bands. Four average spectra of Vero cells, HSV-1 infected Vero cells, HSV-2 infected Vero cells, and VZV infected Vero cells in the 600–1800 cm^{-1} range. All the spectra were manipulated and normalized using OPUS software. The major Raman shifts are labeled in the figure.

doi:10.1371/journal.pone.0153599.g001

Raman shift bands centered at 1315 [50, 57–60] and 1254 cm^{-1} [61] are attributed mainly due to nucleic acids, lipids, and collagen. CH$_2$ and CH functional groups' vibration of lipids and protein respectively, attribute mainly to the band at 1450 cm^{-1} [52, 55]. The peak centered at 1365 cm^{-1} is attributed mainly to tryptophan [56] and guanine [62]. Cytosine contributes to the bands centered at 1284 cm^{-1} [62]. Amide III is represented at this peak, and also at the peaks centered at 1284 [61] and 1238 cm^{-1} [63]. RNA [13] and PO$_2^-$ [57] contribute to the peak centered at 1238 cm^{-1}.

The 1185–1485 cm^{-1} wavenumber region is mainly attributed due to proteins [49, 64], lipids [65], and phosphate compounds [66, 67], via their **CH$_2$, CH$_3$**, and P = O functional groups, respectively.

Carbohydrates and polysaccharides absorption bands contribute mainly in the low wavenumber region below 1185 cm^{-1} [68], due to their functional groups C—O—C, C—O—P.

The major differences between the averages spectra belonging to the four biological systems investigated in this study occur in the high region of the spectrum in 1195–1730 cm^{-1} namely in the proteins ranges amide II and amide III shift bands. Generally, there is a significant reduction in the intensity of absorption at this region as a result of infection with any of the tested viruses.

Fig 2 describes Vero cells viability after infection with HSV-1, HSV-2, and VZV, separately. Vero cell monolayers were separately infected with a high titer (5 m.o.i.) of each one of the
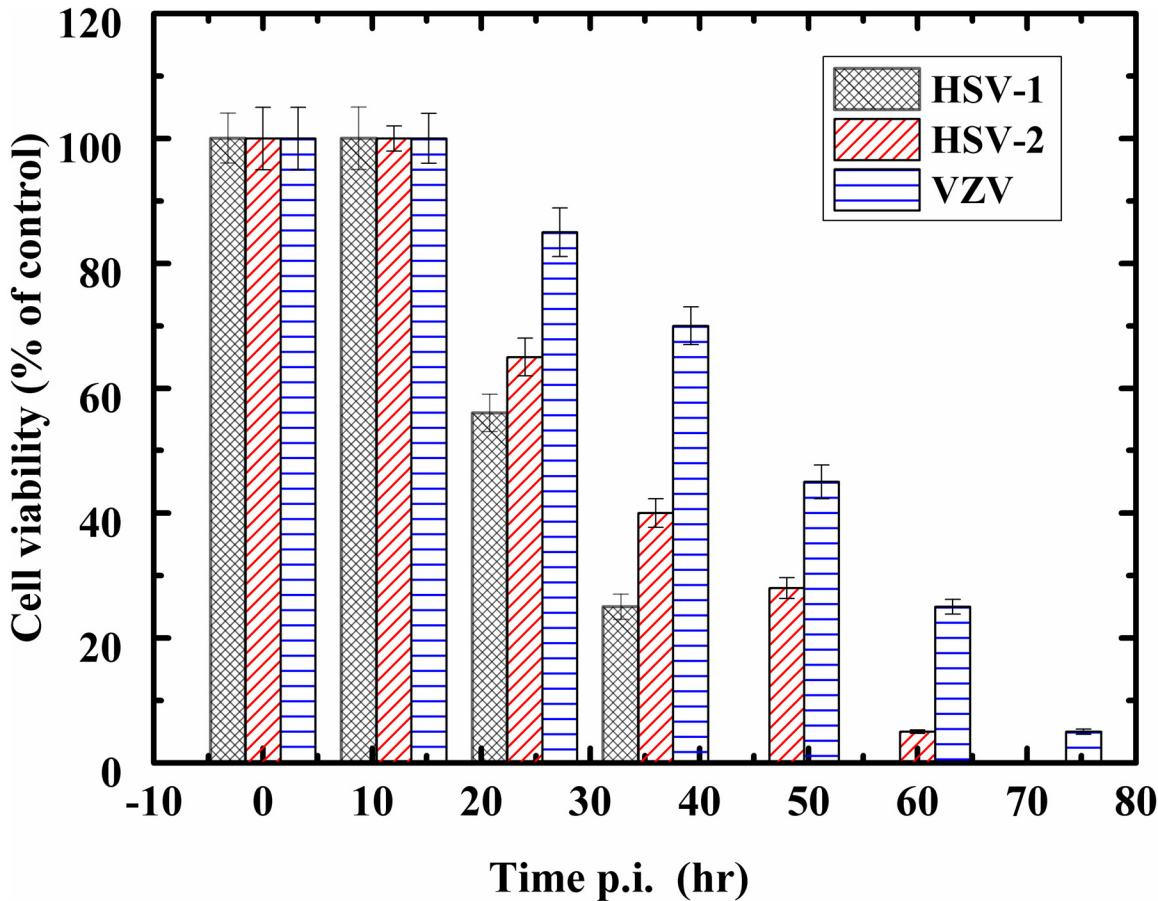
Fig 2. Effect of infection with herpes viruses on cell viability. The effect of infection with the different herpes viruses on cell viability. Vero cell monolayers were infected with 1 m.o.i. of either HSV-1, HSV-2, or VZV. Viability of the infected cells was evaluated at various times post infection (p.i.) by MTT test. Data are mean ± SD (n = 4).

examined viruses and the viability of the infected cells was evaluated at different times post infection, using the MTT test [44]. The results are averages of four different experiments.

As can be seen from the figure, the HSV-1 virus infection manifests itself quicker than infections with the other viruses, with control cell survivability extinguished within 48 hours or less; control cell survivability after HSV-2 and VZV virus infections were reduced to less than 5% after 60 to 72 hours, respectively.

The spectra in Fig 1 are averages spectra. The individual spectra of the four different categories overlap, and that it is difficult to differentiate among them using simple methods like clustering and k-means; thus we used multivariate analysis. Using PCA, we reduced the dimension of the spectra from 688 to 9, making it easier to analyze them using different classifiers. As the purpose of PCA is dimensionality reduction, sometimes it is possible to classify the different categories using projection of the data at different planes, by generating 2D figures. For example, Fig 3 shows 2D plots for: (a) the three infected categories HSV-1, HSV-2 and VZV infected Vero cells, (b) two categories—control cells and HSV-2 infected cells, and (c) two categories—control cells and VZV infected cells. In Fig 3a the HSV-1 infected cells are totally separated from the HSV-2 and VZV infected cells categories, while there are some overlapped points between the HSV-2 and VZV infected cells categories. In Fig 3b, the data points of the two categories; control cells and HSV-2 infected cells are overlapped, and the same trend can be seen
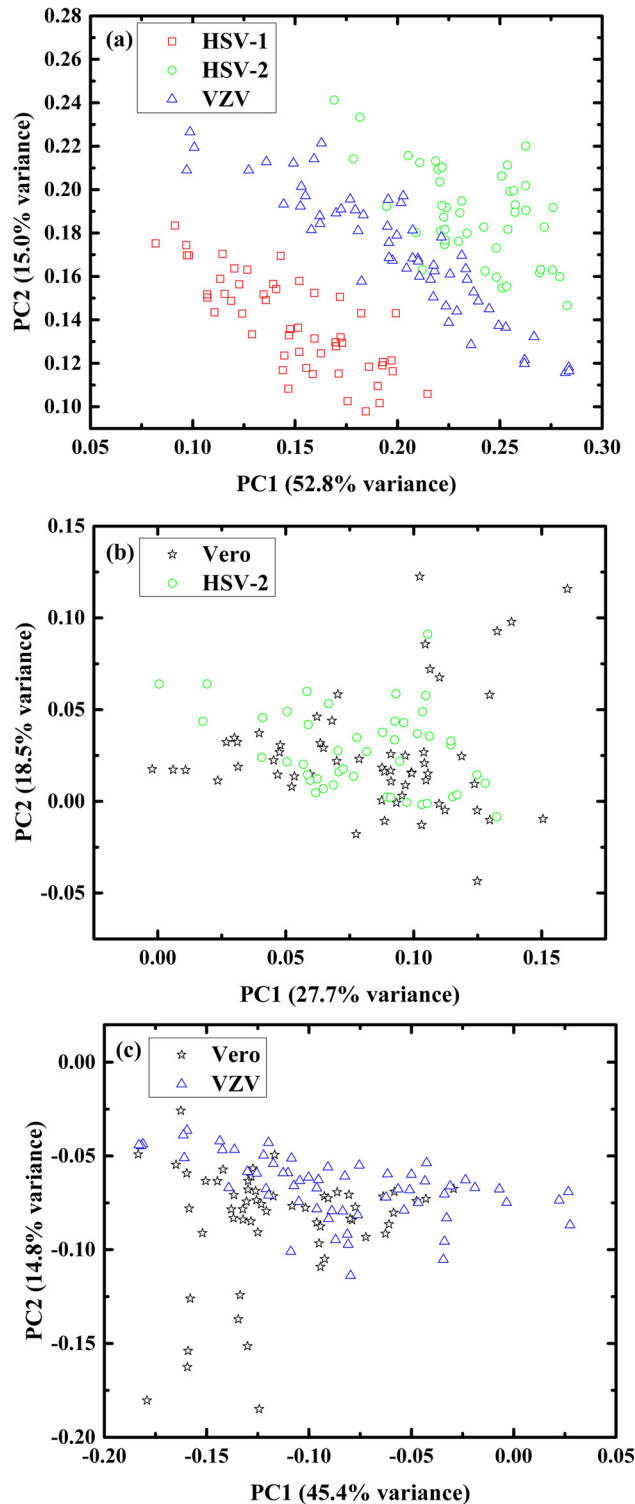
Fig 3. Plotting PC's scores calculated by PCA in two-dimensional plots. 2D figure of the different biological samples investigated in this study. In this figure the scores are shown for PC1 versus PC2: (a) HSV-1 infected Vero cells, HSV-2 infected Vero cells, and VZV infected Vero cells; (b) Vero cells, HSV-2 infected Vero cells; and (c) Vero cells, VZV infected Vero cells.
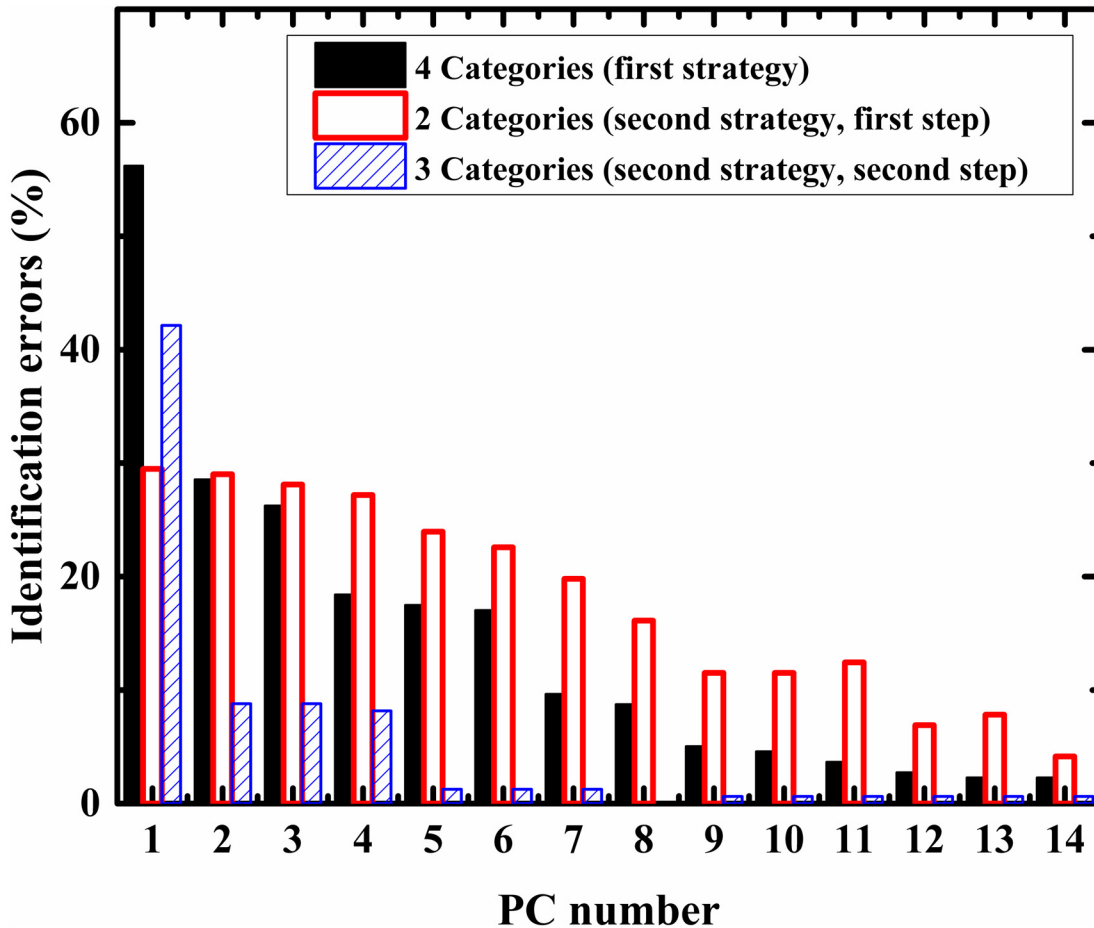
Fig 4. Performance of LDA calculation in different classification procedures. Identification errors, calculated by LDA using LOO algorithm, versus PC number, are presented in the figure. Black squares-the spectra were classified into the four categories of Vero, HSV-1, HSV-2, and VZV simultaneously. Red squares-the spectra were classified into two categories, control and infected. Blue square-the infected spectra were classified into three categories HSV-1, HSV-2 and VZV.

between the control cells and VZV infected cells (Fig 3c). Thus, we used the LDA classifier to classify the four biological systems on the data, after the PCA calculations.

Fig 4 shows identification success in percentage, as a function of PC number. The identification success rates were estimated using the LOO algorithm. This algorithm is usually applied when the statistics are relatively small; here, the training set contained all but one of the measured spectra. The category of this left-out measurement is predicted using LDA and then compared to the known category. This procedure was repeated N times, but in each repetition a different measured spectrum was left out. The classifications were performed using two strategies. In the first strategy, the spectra were classified into four classes; Vero cells, HSV-1 infected Vero cells, HSV-2 infected Vero cells, and VZV infected Vero cells. In the second strategy, the spectra were classified into two steps; in the first step the spectra were classified into two groups, control (Vero cells) and infected cells (HSV-1, HSV-2 and VZV infected Vero cells). In the second step, the spectra of the infected group were classified into three classes: HSV-1 infected Vero cells, HSV-2 infected Vero cells, and VZV infected Vero cells.

As can be seen from Fig 4, for the LOO method to achieve more than 90% accuracy, a different PC number should be used, depending on the strategy chosen; for example using the first

Table 1. Performances of LDA calculations for the first strategy. The calculations were performed in order to differentiate between all four classes—control Vero cells, HSV-1 infected Vero cells, HSV-2 infected Vero cells and VZV infected Vero cells using 13 PCs.

	Vero cells	HSV-1 infected Vero cells	HSV-2 infected Vero cells	VZV infected Vero cells
Vero cells	55		3	
HSV-1 infected Vero cells		53		0
HSV-2 infected Vero cells	1		45	
VZV infected Vero cells	1			59

doi:10.1371/journal.pone.0153599.t001

Table 2. Performances of LDA calculations for the second strategy, step 1: The calculations were performed in order to differentiate between two classes, control Vero cells and infected Vero cells. The infected Vero cells category includes HSV-1 infected Vero cells, HSV-2 infected Vero cells and VZV infected Vero cells, and uses 13 PCs.

	Vero cells	Infected Vero cells
Vero cells	51	7
Infected Vero cells	10	149

doi:10.1371/journal.pone.0153599.t002

strategy (with 4 categories) 8 PCs are needed, while for the second stage step 2, two PCs are needed,

The identification success rates for the first and second strategies are listed in Tables 1 and 2 respectively.

For the second strategy step 2, where the calculations were performed to differentiate among the three sub-classes of the infected category in the first stage of the second strategy, a 100% success rate was achieved using 9 PCs.

We tried to compare between all the different pairs of the four categories: control cells and HSV-1 infected cells; control cells and HSV-2 infected cells; control cells and VZV infected cells; HSV-1 infected cells and HSV-2 infected cells; HSV-1 infected cells and VZV infected cells; and HSV-2 infected cells and VZV infected cells.

The LDA calculations were performed for each pair, using the LOO approach for validation. The results of LDA calculations are presented in Table 3. The success rates of the differentiation among the different groups were calculated using different numbers of PCs.

Analysis of the loadings may give some understanding of spectral features, which may contribute to the discriminant procedure [69, 70]. Using one PC it was possible to differentiate between the control Vero cells and the infected Vero cells with more than a 70% success rate. Thus, it may be suggested that the major bands in PC1 have major roles in the differentiation process (Fig 5). Absolute values of loadings 1 and 2 are shown in Fig 5; the dominant bands are labeled in the figure.

Table 3. Identification success in percentage versus PC number, derived using LDA calculation for six pairs. The cumulative variance is displayed in parentheses.

Number of PCs	Vero cells-HSV-1 infected Vero cells	Vero cells-HSV-2 infected Vero cells	Vero cells-VZV infected Vero cells	HSV-1 infected Vero cells- HSV-2 infected Vero cells	HSV-1 infected Vero cells-VZV infected Vero cells	HSV-2 infected Vero cells-VZV infected Vero cells
PC1	91.9(48.8)	52.9(27.7)	61.0(45.4)	98(52.8)	67.3(48.9)	62.3(46.6)
PC1-PC2	98.2(63.1)	48.1(46.2)	71.2(60.2)	100(67.8)	99.1(67.4)	89.6(60.9)
PC1-PC3	100 (71.6)	65.4(57.3)	77.1(68.6)			88.7(67.9)
PC1-PC4		72.1(64.2)	83.1(72.9)			90.6(73.5)
PC1-PC5		77.9(73.2)	83.9(76.8)			88.7(77.9)
PC1-PC6		91.3(75.8)	91.5(80.1)			99.1(81.1)

doi:10.1371/journal.pone.0153599.t003

Discussion

In our previous study [40], we successfully used Raman spectroscopy to classify HSV-1 infected Vero cells and normal uninfected. In this study, we examined the potential of Raman spectroscopy to identify and classify control uninfected Vero cells and cells infected with either of the three most common members of the herpes virus family (HSV-1, HSV-2, and VZV).

Enlarging the number of categories is a challenge for pattern recognition methods when the classes (tested samples) are very similar. For instance, HSV-1 shares very high similarities with HSV-2, both in their genome sequences (over 70% homology) and in their clinical symptoms [71, 72].

The Raman shifts spectrum is characteristic of the vibrational modes of the biological molecules—protein, nucleic acid, lipid, and carbohydrate molecules, due to their functional groups N—H, C = O, C-H, and P = O vibrations [50, 53, 54, 56–59, 61, 62, 73, 74]. As can be seen from Figs 1 and 5 (PC1), the major spectral differences between the infected Vero cells and the control cells occur in the 1195–1726 cm^{-1} region. Nevertheless, when LDA calculations were performed using the Raman spectra in this region, the performance of these calculations reflected in the classification success rates was slightly decreased when compared to the classification results using the 600–1726 cm^{-1} region. Thus, the 600–1195 cm^{-1} region is still important to the classification procedure. These observations are in accordance with the loading analysis shown in Fig 5. There are some Raman band shifts in the 600–1195 cm^{-1} region (much
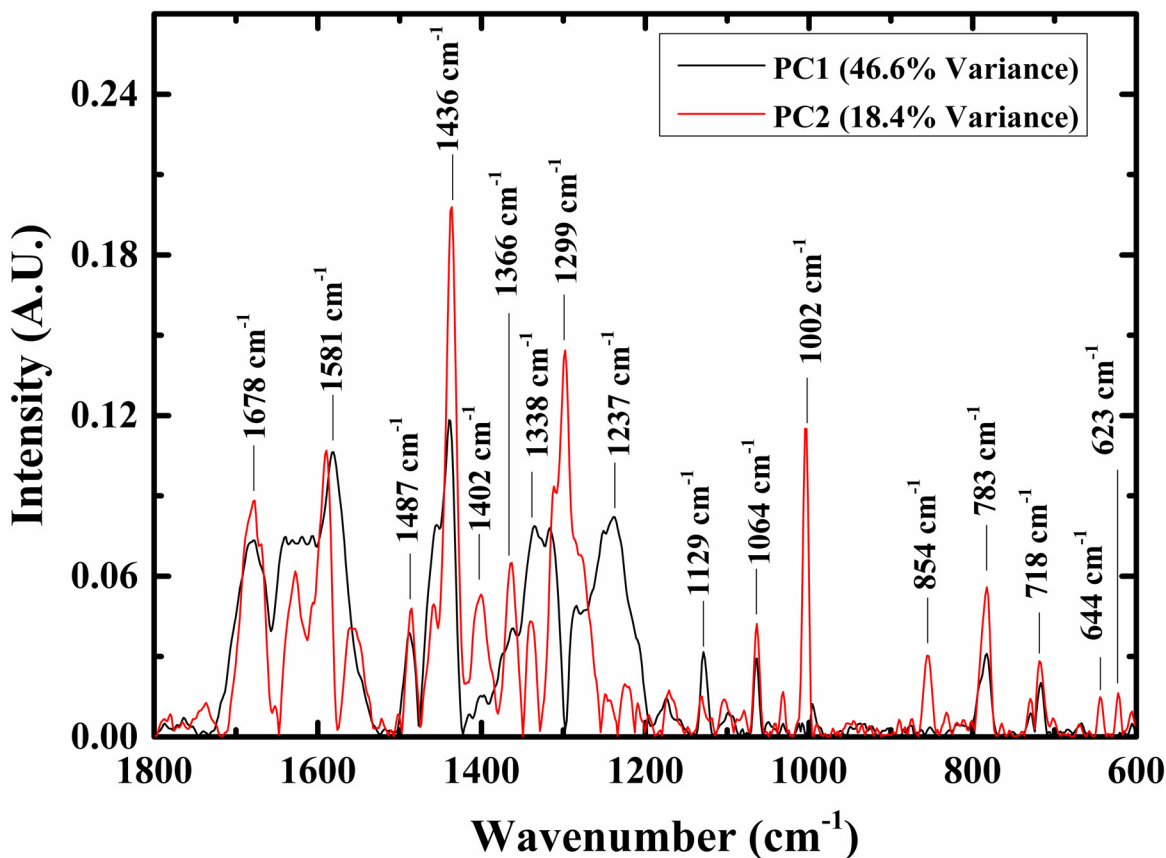

Fig 5. Loadings plots. Loadings 1 and 2 determined using PCA calculations (absolute values) are plotted in the 600–1800 cm^{-1} region. The major peaks and their centroids are displayed in the figure.

smaller than the Raman shifts in the high region); these still could improve the classification performance of the LDA calculation. These band shifts are centered at 1129 cm^{-1}, 1064 cm^{-1}, 783 cm^{-1}, and 718 cm^{-1}, and contributed mainly due to carbohydrates and polysaccharides absorption bands [68], due to their functional groups C—O—C, C—O—P.

As can be seen from Fig 1, the spectral intensities of all infected cells with either of the tested viruses are lower in the 1195–1380 cm^{-1} and 1537–1637 cm^{-1} ranges compared to the control uninfected cells, while they have slightly higher intensities in the 1380–1500 cm^{-1} rang.

The herpes viruses are known as lytic viruses, which cause the termination of all metabolic activities of the host cells after infection, by blocking synthesis of cellular proteins and causing cellular DNA degradation [75, 76]. In fact, these viruses use all cellular stores for their advantage, thereby synthetizing all viral components that are required for their own replication. Thus, infection with these herpes viruses may reduce the amounts of cellular contents such as protein, lipid, and nucleic acid molecules, as reflected in the spectral intensities in Raman shift spectra.

Using PCA the dimensions are reduced to a few PCs (loadings). Each spectrum is represented as a superposition of three loadings (PCs) in the new domain. For example, using five PCs, each spectrum was identified by five numbers named as the coefficients of the loadings. The purpose of PCA calculation is dimensionality reduction, and the projection of the transformed data at certain planes often yields good separation (2D figures) (Fig 3a). For the classification procedure we used the LDA method. The LDA calculation was designed applying the LOO method, which is a common method of cross-validation that has been extensively explored in machine learning and is primarily used to estimate the error in a small sized populations [77, 78]. The classification procedure was performed using two strategies. In the first strategy, the classification was performed among the four biological systems investigated in this study simultaneously. Using 13 PCs it was possible to achieve a classification success rate in excess of 96%. Keeping in mind that the infections with these herpes viruses are biologically similar, these results are considered very good [40, 79–82]. In the second strategy, the classification procedure was performed in two stages. In the first stage the results were classified into two categories, control Vero cells and infected Vero cells. The infected cells include the HSV-1, HSV-2, and VZV infected cells. In this first stage of the second strategy, using 13 PCs made it possible to achieve a classification success rate in excess of 93%.

Applying PC1, the identification errors using two classes of classification, control-infected (second strategy, first stage), were significantly lower than the errors in the four categories classification (first strategy) (Fig 3). This was due to the differences in the number of classes. However, when using more PCs, the trend was changed, which is not surprising, because the intra-variance among the infected group is higher than the intra-variance of each of the four groups. This is because the infected group includes HSV-1, HSV-2, and VZV infected Vero cells.

In the second stage of the second strategy, the infected group was simultaneously distributed into three classes HSV-1 infected cells, HSV-2 infected cells, and VZV infected cells. Using two PCs, it was possible to achieve a classification success rate in excess of 98%.

We tried to compare among the six possible couples of the four biological samples: control cells and HSV-1 infected cells; control cells and HSV-2 infected cells; control cells and VZV infected cells; HSV-1 infected cells and HSV-2 infected cells; HSV-1 infected cells and VZV infected cells; and HSV-2 infected cells and VZV infected cells.

By the nature of PCA, all the data is transformed into a new basis called loadings (PCs), which suggest better classification between the classes. The variance among the classes is captured by the different loadings (PCs). In the new space, each spectrum is calculated as a linear combination of the new basis (loadings). The loadings are arranged in descending order according to their variance; thus, PC1 has the largest variance, followed by PC2, and so on.

As can be seen from Table 3, the largest spectral differences occur between HSV-1 infected cells and HSV-2 infected cells, because when using the first PC1, a 98.0% success rate was achieved. The spectral differences between HSV-1 infected cells and VZV infected cells are also large, because a 99.0% success rate was achieved by using the first two PCs. This result is somewhat surprising because, as mentioned above, HSV-1 and HSV-2 are relatively very close to each other both in their genomes and in their clinical symptoms. More study is required in order to understand the reason for this spectral variance between these viruses. Of course, differences occurred in all different groups because we can differentiate between all the couples and the spectral differences are relative issues

This study proved the potential of Raman spectroscopy as a promising method for successful identification of infected cell cultures with either of the tested herpes viruses. As mentioned in the introduction section, it is highly important to identify the cause of such infections in order to proscribe effective treatment. There are distinct advantages of the Raman spectroscopic method in tandem with multivariate analysis over the classical methods-it takes a short time (few minutes) to determine the cause of the infection and it is highly objective and computerized.

When classification was among the three infected categories, the classification rate was 57.9% using PC1 only, and increased to 91.2% using PC1 and PC2. Thus, we hypothesize that the bands that appear in PC2 but do not appear in PC1 have special importance to the classification procedure among the three infected categories and are listed in Fig 5. The major peaks are centered at 1436 cm^{-1} and contributed mainly to proteins and lipids due to their CH vibrations [52, 55]. Amide III and cytosine are represented at this peak and contributed also to the bands centered at 1299 cm^{-1} [62], while the bands centered at 1002 cm^{-1} are due to phenylalanine in proteins. The bands centered at 854 cm^{-1} are due to DNA [69].

Conclusions

It was possible to differentiate among the infections caused by three different herpes virus types (HSV-1, HSV-2 and VZV) with a high rate of success. This was accomplished through Raman spectroscopy that was analyzed using multivariate analysis. The method is objective, computerized and fast.

Supporting Information

S1 Data. An excel file, "S1 data.xls" was uploaded. This file contains the raw spectral data after spectral manipulations. The file contains four sheets: "Vero" sheet contains the data for the control Vero cells; "HSV1" sheet contains the data for the Vero cells infected with HSV1 virus; "HSV2" sheet contains the data for the Vero cells infected with HSV2 virus and "VZV" sheet contains the data for the Vero cells infected with VZV virus.
(XLS)

Acknowledgments

Author Contributions

Conceived and designed the experiments: AS MH. Performed the experiments: AS MH LZ. Analyzed the data: AS ES MH. Contributed reagents/materials/analysis tools: AS MH LZ ES. Wrote the paper: AS MH ES.

References

1. Gupta R, Warren T, Wald A. Genital herpes. Lancet. 2007; 370(9605):2127–37. doi: 10.1016/S0140-6736(07)61908-4 PMID: 18156035.

2. Markoulatos P, Fountoucidou P, Marinakis G, Krikelis V, Spyrou N, Vamvakopoulos N, et al. Clear detection and typing of herpes simplex virus types 1 and 2 by an indirect ELISA assay: comparison with three different combined methods—capture ELISA, restriction enzymes, and polymerase chain reaction. Journal of clinical laboratory analysis. 1997; 11(3):146–53. PMID: 9138103.

3. Meqdam MM, Todd D, Al-Abosi M. Detection of herpes simplex and varicella zoster viruses in clinical specimens using direct immunofluorescence and cell culture assays. Microbios. 2001; 105(411):111–8. PMID: 11393748.

4. Puppels GJ, de Mul FF, Otto C, Greve J, Robert-Nicoud M, Arndt-Jovin DJ, et al. Studying single living cells and chromosomes by confocal Raman microspectroscopy. Nature. 1990; 347(6290):301–3. doi: 10.1038/347301a0 PMID: 2205805.

5. Wu H, Volponi JV, Oliver AE, Parikh AN, Simmons BA, Singh S. In vivo lipidomics using single-cell Raman spectroscopy. Proceedings of the National Academy of Sciences of the United States of America. 2011; 108(9):3809–14. doi: 10.1073/pnas.1009043108 PMID: 21310969; PubMed Central PMCID: PMC3048102.

6. van Manen HJ, Lenferink A, Otto C. Noninvasive imaging of protein metabolic labeling in single human cells using stable isotopes and Raman microscopy. Analytical chemistry. 2008; 80(24):9576–82. doi: 10.1021/ac801841y PMID: 19006335.

7. Draux F, Jeannesson P, Beljebbar A, Tfayli A, Fourre N, Manfait M, et al. Raman spectral imaging of single living cancer cells: a preliminary study. The Analyst. 2009; 134(3):542–8. doi: 10.1039/b812610k PMID: 19238292.

8. Gniadecka M, Philipsen PA, Sigurdsson S, Wessel S, Nielsen OF, Christensen DH, et al. Melanoma diagnosis by Raman spectroscopy and neural networks: structure alterations in proteins and lipids in intact cancer tissue. The Journal of investigative dermatology. 2004; 122(2):443–9. doi: 10.1046/j.0022-202X.2004.22208.x PMID: 15009728.

9. Haka AS, Shafer-Peltier KE, Fitzmaurice M, Crowe J, Dasari RR, Feld MS. Diagnosing breast cancer by using Raman spectroscopy. Proceedings of the National Academy of Sciences of the United States of America. 2005; 102(35):12371–6. doi: 10.1073/pnas.0501390102 PMID: 16116095; PubMed Central PMCID: PMC1194905.

10. Shafer-Peltier KE, Haka AS, Fitzmaurice M, Crowe J, Myles J, Dasari RR, et al. Raman microspectroscopic model of human breast tissue: implications for breast cancer diagnosis in vivo. Journal of Raman Spectroscopy. 2002; 33(7):552–63. doi: 10.1002/jrs.877

11. Krishna CM, Sockalingum GD, Kurien J, Rao L, Venteo L, Pluot M, et al. Micro-Raman spectroscopy for optical pathology of oral squamous cell carcinoma. Applied spectroscopy. 2004; 58(9):1128–35. doi: 10.1366/0003702041959460 PMID: 15479531.

12. Silveira L Jr., Sathaiah S, Zangaro RA, Pacheco MT, Chavantes MC, Pasqualucci CA. Near-infrared Raman spectroscopy of human coronary arteries: histopathological classification based on Mahalanobis distance. Journal of clinical laser medicine & surgery. 2003; 21(4):203–8. doi: 10.1089/104454703768247774 PMID: 13678457.

13. Chan JW, Taylor DS, Zwerdling T, Lane SM, Ihara K, Huser T. Micro-Raman spectroscopy detects individual neoplastic and normal hematopoietic cells. Biophysical journal. 2006; 90(2):648–56. doi: 10.1529/biophysj.105.066761 PMID: 16239327; PubMed Central PMCID: PMC1367069.

14. Kamemoto LE, Misra AK, Sharma SK, Goodman MT, Luk H, Dykes AC, et al. Near-infrared micro-Raman spectroscopy for in vitro detection of cervical cancer. Applied spectroscopy. 2010; 64(3):255–61. doi: 10.1366/000370210790918364 PMID: 20223058; PubMed Central PMCID: PMC2880181.

15. Keller MD, Kanter EM, Lieber CA, Majumder SK, Hutchings J, Ellis DL, et al. Detecting temporal and spatial effects of epithelial cancers with Raman spectroscopy. Disease markers. 2008; 25(6):323–37. PMID: 19208950; PubMed Central PMCID: PMC2756505.

16. Bodanese B, Silveira L Jr., Albertini R, Zangaro RA, Pacheco MT. Differentiating normal and basal cell carcinoma human skin tissues in vitro using dispersive Raman spectroscopy: a comparison between principal components analysis and simplified biochemical models. Photomedicine and laser surgery. 2010; 28 Suppl 1:S119–27. doi: 10.1089/pho.2009.2565 PMID: 20649423.

17. Lieber CA, Majumder SK, Ellis DL, Billheimer DD, Mahadevan-Jansen A. In vivo nonmelanoma skin cancer diagnosis using Raman microspectroscopy. Lasers in surgery and medicine. 2008; 40(7):461–7. doi: 10.1002/lsm.20653 PMID: 18727020; PubMed Central PMCID: PMC2782422.

18. Huang Y, Swarup VP, Bishnoi SW. Rapid Raman imaging of stable, functionalized nanoshells in mammalian cell cultures. Nano letters. 2009; 9(8):2914–20. doi: 10.1021/nl901234x PMID: 19572746.

19. Mourant JR, Short KW, Carpenter S, Kunapareddy N, Coburn L, Powers TM, et al. Biochemical differences in tumorigenic and nontumorigenic cells measured by Raman and infrared spectroscopy. Journal of biomedical optics. 2005; 10(3):031106. doi: 10.1117/1.1928050 PMID: 16229631.

20. Bergholt MS, Zheng W, Lin K, Ho KY, Teh M, Yeoh KG, et al. Raman endoscopy for in vivo differentiation between benign and malignant ulcers in the stomach. The Analyst. 2010; 135(12):3162–8. doi: 10.1039/c0an00336k PMID: 20941419.

21. Bergholt MS, Zheng W, Lin K, Ho KY, Teh M, Yeoh KG, et al. In vivo diagnosis of gastric cancer using Raman endoscopy and ant colony optimization techniques. International journal of cancer Journal international du cancer. 2011; 128(11):2673–80. doi: 10.1002/ijc.25618 PMID: 20726002.

22. Salman A, Shufan E, Zeiri L, Huleihel M. Detection and identification of cancerous murine fibroblasts, transformed by murine sarcoma virus in culture, using Raman spectroscopy and advanced statistical methods. Biochimica et biophysica acta. 2012. doi: 10.1016/j.bbagen.2012.11.023

23. Feofanov AV, Grichine AI, Shitova LA, Karmakova TA, Yakubovskaya RI, Egret-Charlier M, et al. Confocal raman microspectroscopy and imaging study of theraphthal in living cancer cells. Biophys J. 2000; 78(1):499–512. doi: 10.1016/S0006-3495(00)76612-4 PMID: 10620313; PubMed Central PMCID: PMC1300657.

24. Hawi SR, Nithipatikom K, Wohlfeil ER, Adar F, Campbell WB. Raman microspectroscopy of intracellular cholesterol crystals in cultured bovine coronary artery endothelial cells. Journal of lipid research. 1997; 38(8):1591–7. PMID: 9300781.

25. Verma SP, Schmidt-Ullrich R, Thompson WS, Wallach DF. Differences between the structural dynamics of plasma membranes of normal hamster lymphocytes and lymphoid cells neoplastically transformed by simian virus 40 as revealed by laser Raman spectroscopy. Cancer research. 1977; 37 (10):3490–3. PMID: 198115.

26. Ellis DI, Goodacre R. Metabolic fingerprinting in disease diagnosis: biomedical applications of infrared and Raman spectroscopy. The Analyst. 2006; 131(8):875–85. doi: 10.1039/b602376m PMID: 17028718.

27. Smith E, Dent G. Modern Raman Spectroscopy: A Practical Approach: Wiley; 2005.

28. Krafft C. Bioanalytical applications of Raman spectroscopy. Analytical and bioanalytical chemistry. 2004; 378(1):60–2. doi: 10.1007/s00216-003-2266-6 PMID: 14576969.

29. Matthaus C, Boydston-White S, Miljkovic M, Romeo M, Diem M. Raman and infrared microspectral imaging of mitotic cells. Applied spectroscopy. 2006; 60(1):1–8. doi: 10.1366/000370206775382758 PMID: 16454901; PubMed Central PMCID: PMC2732123.

30. Kazanci M, Roschger P, Paschalis EP, Klaushofer K, Fratzl P. Bone osteonal tissues by Raman spectral mapping: orientation-composition. Journal of structural biology. 2006; 156(3):489–96. doi: 10.1016/j.jsb.2006.06.011 PMID: 16931054.

31. Notingher I, Boccaccini AR, Jones J, Maquet V, Hench LL. Application of Raman microspectroscopy to the characterisation of bioactive materials. Materials Characterization. 2002; 49(3):255–60. doi: 10.1016/S1044-5803(03)00029-9

32. Carter EA, Edwards HG. Biological Applications oI Raman Spectroscopy. Infrared and Raman spectroscopy of biological materials. 2001; 24:421.

33. Mariani MM, Maccoux LJ, Matthaus C, Diem M, Hengstler JG, Deckert V. Micro-Raman detection of nuclear membrane lipid fluctuations in senescent epithelial breast cancer cells. Analytical chemistry. 2010; 82(10):4259–63. doi: 10.1021/ac1006987 PMID: 20380478.

34. Zonios GI, Cothren RM, Arendt JT, Wu J, Van Dam J, Crawford JM, et al. Morphological model of human colon tissue fluorescence. IEEE transactions on bio-medical engineering. 1996; 43(2):113–22. doi: 10.1109/10.481980 PMID: 8682522.

35. Georgakoudi I, Jacobson BC, Muller MG, Sheets EE, Badizadegan K, Carr-Locke DL, et al. NAD(P)H and collagen as in vivo quantitative fluorescent biomarkers of epithelial precancerous changes. Cancer research. 2002; 62(3):682–7. PMID: 11830520.

36. Mourant JR, Yamada YR, Carpenter S, Dominique LR, Freyer JP. FTIR spectroscopy demonstrates biochemical differences in mammalian cell cultures at different growth stages. Biophysical journal. 2003; 85(3):1938–47. doi: 10.1016/S0006-3495(03)74621-9 PMID: 12944306; PubMed Central PMCID: PMC1303365.

37. Diem M, Chiriboga L, Yee H. Infrared spectroscopy of human cells and tissue. VIII. Strategies for analysis of infrared tissue mapping data and applications to liver tissue. Biopolymers. 2000; 57(5):282–90. doi: 10.1002/1097-0282(2000)57:5<282::AID-BIP50>3.0.CO;2-R PMID: 10958320.

38. Argov S, Ramesh J, Salman A, Sinelnikov I, Goldstein J, Guterman H, et al. Diagnostic potential of Fourier-transform infrared microspectroscopy and advanced computational methods in colon cancer patients. J Biomed Opt. 2002; 7(2):248–54. doi: 10.1117/1.1463051 PMID: 11966311.

39. Salman A, Argov S, Ramesh J, Goldstein J, Sinelnikov I, Guterman H, et al. FT-IR microscopic characterization of normal and malignant human colonic tissues. Cell Mol Biol (Noisy-le-grand). 2001; 47 Online Pub:OL159-66. PMID: 11936863.

40. Salman A, Shufan E, Zeiri L, Huleihel M. Characterization and detection of Vero cells infected with Herpes Simplex Virus type 1 using Raman spectroscopy and advanced statistical methods. Methods. 2014; 68(2):364–70. doi: 10.1016/j.ymeth.2014.02.022 PMID: 24582780.

41. Salman A, Ramesh J, Erukhimovitch V, Talyshinsky M, Mordechai S, Huleihel M. FTIR microspectroscopy of malignant fibroblasts transformed by mouse sarcoma virus. J Biochem Biophys Methods. 2003; 55(2):141–53. PMID: 12628697.

42. Erukhimovitch V, Talyshinsky M, Souprun Y, Huleihel M. Spectroscopic characterization of human and mouse primary cells, cell lines and malignant cells. Photochemistry and photobiology. 2002; 76 (4):446–51. PMID: 12405154.

43. Huleihel M, Ishanu V, Tal J, Arad SM. Antiviral effect of red microalgal polysaccharides on Herpes simplex and Varicella zoster viruses. Journal of applied phycology. 2001; 13(2):127–34.

44. Shi Y, Kornovski BS, Savani R, Turley EA. A rapid, multiwell colorimetric assay for chemotaxis. Journal of immunological methods. 1993; 164(2):149–54. PMID: 8370922.

45. Bishop CM. Pattern recognition and machine learning. New York: Springer; 2006. xx, 738 p. p.

46. Duda RO, Hart PE, Stork DG. Pattern classification: Wiley; 2001.

47. Salman A, Lapidot I, Pomerantz A, Tsror L, Shufan E, Moreh R, et al. Identification of fungal phytopathogens using Fourier transform infrared-attenuated total reflection spectroscopy and advanced statistical methods. J Biomed Opt. 2012; 17(1):017002. doi: 10.1117/1.JBO.17.1.017002 PMID: 22352668.

48. Salman A, Shufan E, Zeiri L, Huleihel M. Detection and identification of cancerous murine fibroblasts, transformed by murine sarcoma virus in culture, using Raman spectroscopy and advanced statistical methods. Biochim Biophys Acta. 2013; 1830(3):2720–7. PMID: 23671933.

49. Kos G, Lohninger H, Krska R. Development of a method for the determination of Fusarium fungi on corn using mid-infrared spectroscopy with attenuated total reflection and chemometrics. Analytical chemistry. 2003; 75(5):1211–7. PMID: 12641243.

50. Stone N, Kendall C, Smith J, Crow P, Barr H. Raman spectroscopy for identification of epithelial cancers. Faraday discussions. 2004; 126:141–57; discussion 69–83. PMID: 14992404.

51. Faolain EO, Hunter MB, Byrne JM, Kelehan P, Lambkin HA, Byrne HJ, et al. Raman spectroscopic evaluation of efficacy of current paraffin wax section dewaxing agents. The journal of histochemistry and cytochemistry: official journal of the Histochemistry Society. 2005; 53(1):121–9. PMID: 15637345.

52. Naumann D, editor Infrared and NIR Raman spectroscopy in medical microbiology. Proceedings of SPIE (1998); Washington: Bellingham.

53. Agarwal R, Tandon P, Gupta VD. Phonon dispersion in poly(dimethylsilane). Journal of Organometallic Chemistry. 2006; 691(13):2902–8. doi: 10.1016/j.jorganchem.2006.02.032

54. Shaw RA, Mantsch HH. Vibrational biospectroscopy: from plants to animals to humans. A historical perspective. Journal of Molecular Structure. 1999; 480–481(0):1–13. doi: 10.1016/S0022-2860(98)00648-6

55. Huang Z, McWilliams A, Lui H, McLean DI, Lam S, Zeng H. Near-infrared Raman spectroscopy for optical diagnosis of lung cancer. International journal of cancer Journal international du cancer. 2003; 107 (6):1047–52. doi: 10.1002/ijc.11500 PMID: 14601068.

56. Cheng W-T, Liu M-T, Liu H-N, Lin S-Y. Micro-Raman spectroscopy used to identify and grade human skin pilomatrixoma. Microscopy Research and Technique. 2005; 68(2):75–9. doi: 10.1002/jemt.20229 PMID: 16228983.

57. Stone N, Kendall C, Shepherd N, Crow P, Barr H. Near-infrared Raman spectroscopy for the classification of epithelial pre-cancers and cancers. Journal of Raman Spectroscopy. 2002; 33(7):564–73. doi: 10.1002/jrs.882

58. Min Y-K, Yamamoto T, Kohda E, Ito T, Hamaguchi H-o. 1064 nm near-infrared multichannel Raman spectroscopy of fresh human lung tissues. Journal of Raman Spectroscopy. 2005; 36(1):73–6. doi: 10.1002/jrs.1280

59. Farquharson S, Shende C, Inscore FE, Maksymiuk P, Gift A. Analysis of 5-fluorouracil in saliva using surface-enhanced Raman spectroscopy. Journal of Raman Spectroscopy. 2005; 36(3):208–12. doi: 10.1002/jrs.1277

60. Lau DP, Huang Z, Lui H, Man CS, Berean K, Morrison MD, et al. Raman spectroscopy for optical diagnosis in normal and cancerous tissue of the nasopharynx—preliminary findings. Lasers in Surgery and Medicine. 2003; 32(3):210–4. doi: 10.1002/lsm.10084 PMID: 12605428.

61. Dukor RK. Vibrational Spectroscopy in the Detection of Cancer. Handbook of Vibrational Spectroscopy: John Wiley & Sons, Ltd; 2006.

62. Ruiz-Chica AJ, Medina MA, Sánchez-Jiménez F, Ramírez FJ. Characterization by Raman spectroscopy of conformational changes on guanine—cytosine and adenine—thymine oligonucleotides induced by aminooxy analogues of spermidine. Journal of Raman Spectroscopy. 2004; 35(2):93–100. doi: 10.1002/jrs.1107

63. Ó Faoláin E, Hunter MB, Byrne JM, Kelehan P, McNamara M, Byrne HJ, et al. A study examining the effects of tissue processing on human tissue sections using vibrational spectroscopy. Vibrational Spectroscopy. 2005; 38(1–2):121–7. doi: 10.1016/j.vibspec.2005.02.013

64. Eckel R, Huo H, Guan H-W, Hu X, Che X, Huang W-D. Characteristic infrared spectroscopic patterns in the protein bands of human breast cancer tissue. Vibrational Spectroscopy. 2001; 27(2):165–73. doi: 10.1016/S0924-2031(01)00134-5

65. Fujioka N, Morimoto Y, Arai T, Kikuchi M. Discrimination between normal and malignant human gastric tissues by Fourier transform infrared spectroscopy. Cancer Detection and Prevention. 2004; 28(1):32–6. doi: 10.1016/j.cdp.2003.11.004 PMID: 15041075

66. Yoshida S, Miyazaki M, Sakai K, Takeshita M, Yuasa S, Sato A, et al. Fourier transform infrared spectroscopic analysis of rat brain microsomal membranes modified by dietary fatty acids: Possible correlation with altered learning behavior. Biospectroscopy. 1997; 3(4):281–90. doi: 10.1002/(SICI)1520-6343(1997)3:4<281::AID-BSPY3>3.0.CO;2-7

67. Dovbeshko GI, Chegel VI, Gridina NY, Repnytska OP, Shirshov YM, Tryndiak VP, et al. Surface enhanced IR absorption of nucleic acids from tumor cells: FTIR reflectance study. Biopolymers. 2002; 67(6):470–86. doi: 10.1002/bip.10165 PMID: 12209454

68. Naumann A. A novel procedure for strain classification of fungal mycelium by cluster and artificial neural network analysis of Fourier transform infrared (FTIR) spectra. The Analyst. 2009; 134(6):1215–23. doi: 10.1039/b821286d PMID: 19475151.

69. Moor K, Ohtani K, Myrzakozha D, Zhanserkenova O, Andriana BB, Sato H. Noninvasive and label-free determination of virus infected cells by Raman spectroscopy. J Biomed Opt. 2014; 19(6):067003. doi: 10.1117/1.JBO.19.6.067003 PMID: 24898605.

70. Salman A, Shufan E, Sahu RK, Mordechai S, Sebbag G. Insights on colorectal cancer relapse by infrared microscopy from anastomosis tissues: Further analysis. Vibrational Spectroscopy. 2016; 83:17–25. doi: 10.1016/j.vibspec.2016.01.002

71. Eberle R, Courtney RJ. Topological distribution of virus-specific and cross-reactive antigenic determinants on the gB glycoprotein of the herpes simplex viruses. J Med Virol. 1989; 27(4):309–16. PMID: 2470853.

72. Chayavichitsilp P, Buckwalter JV, Krakowski AC, Friedlander SF. Herpes simplex. Pediatr Rev. 2009; 30(4):119–29; quiz 30. doi: 10.1542/pir.30-4-119 PMID: 19339385.

73. Chan JW, Taylor DS, Zwerdling T, Lane SM, Ihara K, Huser T. Micro-Raman Spectroscopy Detects Individual Neoplastic and Normal Hematopoietic Cells. Biophysical Journal. 2006; 90(2):648–56. doi: 10.1529/biophysj.105.066761 PMID: 16239327

74. Schulz H, Baranska M. Identification and quantification of valuable plant substances by IR and Raman spectroscopy. Vibrational Spectroscopy. 2007; 43(1):13–25. doi: 10.1016/j.vibspec.2006.06.001

75. Erukhimovitch V, Bogomolny E, Huleihil M, Huleihel M. Infrared spectral changes identified during different stages of herpes viruses infection in vitro. The Analyst. 2011; 136(13):2818–24. doi: 10.1039/c1an15319f PMID: 21611647.

76. Vogel R, Seyffert M, Strasser R, de Oliveira AP, Dresch C, Glauser DL, et al. Adeno-associated virus type 2 modulates the host DNA damage response induced by herpes simplex virus 1 during coinfection. Journal of virology. 2012; 86(1):143–55. doi: 10.1128/JVI.05694-11 PMID: 22013059; PubMed Central PMCID: PMC3255894.

77. Evgeniou T, Pontil M, Elisseeff A. Leave One Out Error, Stability, and Generalization of Voting Combinations of Classifiers. Machine Learning. 2004; 55(1):71–97. doi: 10.1023/B:MACH.0000019805.88351.60

78. Elisseeff A, Pontil M. Leave-one-out Error and Stability of Learning Algorithms with Applications. In: Suykens J, Horvath G, Basu S, Micchelli C, Vandewalle J, editors. Learning Theory and Practice: IOS Press; 2002.

79. Salman A, Shufan E, Lapidot I, Tsror L, Moreh R, Mordechai S, et al. Assignment of Colletotrichum coccodes isolates into vegetative compatibility groups using infrared spectroscopy: a step towards practical application. Analyst. 2015; 140(9):3098–106. doi: 10.1039/c5an00213c PMID: 25790802.

80. Salman A, Sebbag G, Argov S, Mordechai S, Sahu RK. Early detection of colorectal cancer relapse by infrared spectroscopy in "normal" anastomosis tissue. J Biomed Opt. 2015; 20(7):75007. doi: 10.1117/1.JBO.20.7.075007 PMID: 26178200.

81. Salman A, Shufan E, Tsror L, Moreh R, Mordechai S, Huleihel M. Classification of Colletotrichum coccodes isolates into vegetative compatibility groups using infrared attenuated total reflectance spectroscopy and multivariate analysis. Methods. 2014; 68(2):325–30. doi: 10.1016/j.ymeth.2014.02.021 PMID: 24582779.

82. Pomerantz A, Cohen Y, Shufan E, Ben-Naim Y, Mordechai S, Salman A, et al. Characterization of Phytophthora infestans resistance to mefenoxam using FTIR spectroscopy. J Photochem Photobiol B. 2014; 141:308–14. doi: 10.1016/j.jphotobiol.2014.10.005 PMID: 25463683.